A Pathched-Grid Algorithm for Complex Aircraft Configurations*

Robert W. Walters†
James L. Thomas**

Abstract. A patched-grid algorithm for the analysis of complex configurations with an implicit, upwind-biased Navier-Stokes solver is presented. Through the use of a generalized coordinate transformation at the zonal interface between two or more blocks, the algorithm can be applied to highly stretched viscous grids and to arbitrarily-shaped patch boundaries. Applications are made to the SR71 reconnaissance aircraft in a high-altitude enviroment at a supersonic speed and to the F/A-18 forebody-strake configuration at subsonic, high-alpha conditions, in support of the NASA High-Alpha Research Program.

1. Introduction. There is an increasing effort in the development and application of Euler/Navier-Stokes computational algorithms for realistic aircraft configurations. The present work is directed toward the development of improved techniques associated with the block structured approach, and in particular the patched grid approach. In this method, also referred to as a domain decomposition method, the computational domain is divided into a number of zones or blocks, each of which models the local geometric features and requisite physics of the configuration [1-8]. The grids in each zone can be determined independently, with the net result that the grid generation task is simpler and the solution is more efficient, since local clustering of the grid cells to resolve geometric and physical features in one region need not propagate to other blocks. The method is extended in the present work so that the patching plane can be a general three-dimensional surface. The extension also overcomes a problem encountered in the application to viscous flows, in which a highly stretched grid is present on either side of a zonal interface.

2. Governing Equations. The governing equations are the thin–layer approximations to the three–dimensional, time–dependent, compressible Navier–Stokes equations, written in generalized coordinates and conservation law form as

$$\frac{\partial \hat{Q}}{\partial t} + \frac{\partial \hat{F}}{\partial \xi} + \frac{\partial \hat{G}}{\partial \eta} + \frac{\partial (\hat{H} - \hat{H}_v)}{\partial \zeta} = 0 \tag{2.1a}$$

$$\hat{Q} = \frac{Q}{J} = \frac{1}{J}\begin{bmatrix} \rho \\ \rho u \\ \rho v \\ \rho w \\ e \end{bmatrix} \qquad \hat{F} = \frac{1}{J}\begin{bmatrix} \rho U \\ \rho U u + \xi_x p \\ \rho U v + \xi_y p \\ \rho U w + \xi_z p \\ (e+p)U \end{bmatrix} \tag{2.1b}$$

*The work of the first author was supported by the NASA Langley Research Center.

†Department of Aerospace and Ocean Engineering, Virginia Polytechnic Institute and State University, Blacksburg, VA 24061.

**Fluid Mechanics Division, NASA Langley Research Center, Hampton, VA 23665.

$$\widehat{G} = \frac{1}{J}\begin{bmatrix} \rho V \\ \rho V u + \eta_x p \\ \rho V v + \eta_y p \\ \rho V w + \eta_z p \\ (e+p)V \end{bmatrix} \qquad \widehat{H} = \frac{1}{J}\begin{bmatrix} \rho W \\ \rho W u + \zeta_x p \\ \rho W v + \zeta_y p \\ \rho W w + \zeta_z p \\ (e+p)W \end{bmatrix} \tag{2.1c}$$

$$\widehat{H}_v = \frac{1}{J}\begin{bmatrix} 0 \\ \zeta_x \tau_{xx} + \zeta_y \tau_{xy} + \zeta_z \tau_{xz} \\ \zeta_x \tau_{xy} + \zeta_y \tau_{yy} + \zeta_z \tau_{yz} \\ \zeta_x \tau_{xz} + \zeta_y \tau_{yz} + \zeta_z \tau_{zz} \\ \zeta_x b_x + \zeta_y b_y + \zeta_z b_z \end{bmatrix} \tag{2.1d}$$

$$\begin{aligned} U &= \xi_x u + \xi_y v + \xi_z w \\ V &= \eta_x u + \eta_y v + \eta_z w \\ W &= \zeta_x u + \zeta_y v + \zeta_z w \end{aligned} \tag{2.1e}$$

A general three–dimensional transformation between the Cartesian variables (x,y,z) and the generalized coordinates (ξ, η, ζ) is implied in (2.1), where ζ corresponds to the coordinate normal to the body surface. The vector Q represents density, momentum, and total energy per unit volume and p is the pressure defined from the equation of state for an ideal gas.

$$p = (\gamma - 1)(e - \rho(u^2 + v^2 + w^2)/2) \tag{2.2}$$

The shear stress and heat flux terms are defined in tensor notation (summation convention implied) as:

$$\tau_{x_i x_j} = \frac{M_\infty}{Re_L}\left[\mu\left(\frac{\partial u_i}{\partial x_j} + \frac{\partial u_j}{\partial x_i}\right) + \lambda \frac{\partial u_k}{\partial x_k}\delta_{ij}\right] \tag{2.3}$$

$$\dot{q}_{x_i} = -\left(\frac{M_\infty}{Re_L \sigma(\gamma - 1)}\right)\frac{\partial c^2}{\partial x_i}, \quad b_{x_i} = u_j \tau_{x_i x_j} - \dot{q}_{x_i} \tag{2.4}$$

where σ is Prandtl number, M is Mach number, and Re_L is Reynolds number evaluated at freestream conditions based on a characteristic body length. The equations are nondimensionalized with reference values of length, density, speed of sound, and viscosity, i.e. L^*, ρ^*_∞, c^*_∞, and μ^*_∞, respectively. The chain rule is used to evaluate derivatives with respect to (x,y,z) in terms of (ξ, η, ζ). Consistent with the thin–layer assumption, only those derivatives in the direction normal to the wall (ζ) are retained in the shear stress and heat flux terms. For laminar flow, (2.1) is closed by Stokes hypothesis for bulk viscosity ($\lambda + 2\mu/3 = 0$) and Sutherland's law for molecular viscosity. The effect of turbulence is accounted for through the concepts of an eddy viscosity and eddy conductivity. The algebraic turbulence model of Baldwin and Lomax [9] is used to evaluate the turbulence quantities including the modifications introduced by Degani-Schiff [10] to ensure the proper length scales are used in separated vortical flows.

The governing equations, while written in generalized curvilinear coordinates, are solved in a finite-volume formulation. The finite-difference solution to the fluid dynamic equations in strong conservation form in a transformed space is equivalent to the solution of a finite-volume algorithm, subject to proper interpretation of the metric derivatives. The ratio of the metric derivatives to the Jacobian J is taken to be the appropriate projected area of cell faces and the reciprocal of the Jacobians is taken to be the cell volumes [11]. Such an approach then honors the geometric conservation law such that the discrete equations are satisfied identically when evaluated at freestream conditions on an arbitrary mesh.

3. Numerical Algorithm. The generalized fluxes $\widehat{F}, \widehat{G}, \widehat{H}$, representing pressure and convection terms, are upwind differenced with the flux-difference splitting of Roe [12,13]. The spatial derivatives are written conservatively as a flux balance across a cell as, for example, holding spatial indices i and j constant

$$(\frac{\partial \widehat{H}}{\partial \zeta})_k = \frac{\widehat{H}_{k+1/2} - \widehat{H}_{k-1/2}}{\zeta_{k+1/2} - \zeta_{k-1/2}} \tag{3.1}$$

where the subscript k refers to a cell-centered location (ξ_i, η_j, ζ_k) and $k+1/2$ corresponds to a cell-interface location $(\xi_i, \eta_j, \zeta_{k+1/2})$. The interface flux is determined from a state-variable interpolation and a locally one-dimensional model of wave interactions normal to the cell interfaces [14,15] and can be written as

$$\widehat{H}_{k+1/2} = \frac{1}{2}\left[\, \widehat{H}(Q_L) + \widehat{H}(Q_R) - |\tilde{C}|\,(Q_R - Q_L) \,\right]_{k+1/2} \tag{3.2}$$

which corresponds to the exact solution of an approximate Riemann problem, where $|\tilde{C}| = \tilde{T}\,|\tilde{\Lambda}|\,\tilde{T}^{-1}$ is evaluated with Roe-averaged variables such that $\widehat{H}_R - \widehat{H}_L = \tilde{C}\,(Q_R - Q_L)$ is satisfied exactly.

The state-variable interpolations determine the accuracy of the scheme. The state variable at the interface is constructed from nonoscillatory interpolation [14] of the primitive variables where higher order accurate differencing is given by a one-parameter family

$$\begin{aligned}(Q_L)_{k+1/2} &= Q_k + \frac{1}{4}\left[(1-\kappa)\overline{\nabla}Q + (1+\kappa)\overline{\Delta}Q\right]_k \\ (Q_R)_{k+1/2} &= Q_{k+1} - \frac{1}{4}\left[(1+\kappa)\overline{\nabla}Q + (1-\kappa)\overline{\Delta}Q\right]_{k+1}\end{aligned} \tag{3.3}$$

where $\overline{\nabla}Q$ and $\overline{\Delta}Q$ are backward and forward differences of Q, respectively, which are limited, using the min-mod limiter described in [15], to ensure monotone interpolation across discontinuities in the solution, such as shock waves. For all of the results presented, the third-order discretization corresponding to $\kappa = 1/3$ is used.

The thin-layer approximations to the shear stress and heat-transfer terms are contained in $\widehat{H}_v$ and are centrally differenced. Second derivatives are treated as differences across cell interfaces of first derivative terms, as below, holding spatial indices i and j constant

$$\delta_\zeta \widehat{H}_{v_k} = \widehat{H}_{v_{k+1/2}} - \widehat{H}_{v_{k-1/2}} \tag{3.4}$$

The term $H_{v_{k+1/2}}$ is defined as below

$$\widehat{H}_v = \frac{M_\infty \mu}{Re_L J}\begin{bmatrix} 0 \\ \phi_1 u_\zeta + \zeta_x \phi_2 \\ \phi_1 v_\zeta + \zeta_y \phi_2 \\ \phi_1 w_\zeta + \zeta_z \phi_2 \\ \phi_1[(\frac{q^2}{2})_\zeta + \frac{1}{\sigma(\gamma-1)}(c^2)_\zeta] + W\phi_2 \end{bmatrix} \tag{3.5a}$$

where

$$\phi_1 = \zeta_x^2 + \zeta_y^2 + \zeta_z^2 \tag{3.5b}$$

$$\phi_2 = (\zeta_x u_\zeta + \zeta_y v_\zeta + \zeta_z w_\zeta)/3 \tag{3.5c}$$

and $\delta_\zeta u_{k+1/2} = u_{k+1} - u_k$. Implemented in a finite volume approach, the above formula requires an approximation to the volume at the cell interface $(1/J)_{k+1/2}$ which is calculated by averaging the neighboring values.

Analysis of the dissipation arising from the above algorithm is presented by Van Leer et. al [13] which indicates that the flux-difference splitting approach takes accounts of all the ways through which neighboring cells interact and thus resolves well in the steady state both shocks and contact discontinuities. This is in contrast to the flux-vector splitting approach in which only steady shocks are resolved well. Hence, boundary layers are resolved more accurately with the former approach, as substantiated by the numerical computations [13]. A comparison of the flux-difference splitting approach to a central difference scheme with explicitly added dissipation for a series of viscous flows is presented by Vatsa et. al. [11]. The results indicate that the simpler scalar dissipation in the central difference scheme needs to be reduced in the boundary layers for the results to be

comparable. The dissipation was reduced in [11] by multiplying by the magnitude of the local Mach number, although other approaches are possible.

In order to advance the equations in time, the linearized, backward–Euler approximation in delta form for the three–dimensional equations is used which is given as

$$\left[\frac{I}{J\Delta t}+\delta_\xi\frac{\partial\widehat{F}}{\partial Q}+\delta_\eta\frac{\partial\widehat{G}}{\partial Q}+\delta_\zeta\left(\frac{\partial\widehat{H}-\partial\widehat{H}_v}{\partial Q}\right)\right]\Delta Q=-L(Q^n) \tag{3.6}$$

where $L(Q^n)$ is the discrete representation of the spatial derivative terms in (2.1) evaluated at time level n. The above equation is either spatially factored and solved as a series of three sweeps through the mesh i.e.,

$$\begin{aligned}
&\left[\frac{I}{J\Delta t}+\delta_\xi\frac{\partial\widehat{F}}{\partial Q}\right]\Delta Q^*=-L(Q^n)\\
&\left[\frac{I}{J\Delta t}+\delta_\eta\frac{\partial\widehat{G}}{\partial Q}\right]\Delta Q^{**}=\left(\frac{I}{J\Delta t}\right)\Delta Q^*\\
&\left[\frac{I}{J\Delta t}+\delta_\zeta\left(\frac{\partial\widehat{H}-\partial H_v}{\partial Q}\right)\right]\Delta Q=\left(\frac{I}{J\Delta t}\right)\Delta Q^{**}
\end{aligned} \tag{3.7}$$

or solved by a two sweep hybrid relaxation/approximate-factorization procedure which utilizes a non-linear update of the residual given as

$$\begin{aligned}
&\left[M+\delta_\eta\frac{\partial\widehat{G}}{\partial Q}\right]\Delta Q^*=-L(Q^n,Q^{n+1})\\
&\left[M+\delta_\zeta\left(\frac{\partial\widehat{H}-\partial H_v}{\partial Q}\right)\right]\Delta Q=M\Delta Q^*
\end{aligned} \tag{3.8a}$$

where

$$M=\left[\frac{I}{J\Delta t}+\frac{\partial\widehat{F}^+}{\partial Q}-\frac{\partial\widehat{F}^-}{\partial Q}\right] \tag{3.8b}$$

Both algorithms are followed by the update step

$$Q^{n+1}=Q^n+\Delta Q \tag{3.9}$$

The algorithms are written in delta form so that the steady–state solutions are independent of the time step Δt.

The implicit spatial derivatives of the convective and pressure terms are first order accurate, leading to block tridiagonal inversions for each sweep. The algorithms are conditionally stable and optimal convergence is obtained with a spatially varying time step corresponding to a Courant number on the order of ten. The operations are completely vectorizable, the smallest vector lengths being encountered in the matrix inversions. The inversions in η, for example, are recursive and not vectorizable in η but are vectorized over the other direction(s).

4. Patching Algorithm. The two general approaches considered for patching across zonal grids with coincident boundaries can be addressed based on the sketch in Fig. 1. Two-dimensional Cartesian grids in two zones are shown; the two zones have uniform spacing in the x-direction and a grid mismatch in the y-direction. The indices (i,j) refer to the cell-center locations of zone 1 and (l,m) to those of zone 2. The zonal interface across which the solution must be patched corresponds to the points defined as $\{x_{i+1/2,j}\,;j=1,j_{max}\}$ and $\{x_{l-1/2,m}\,;m=1,m_{max}\}$.

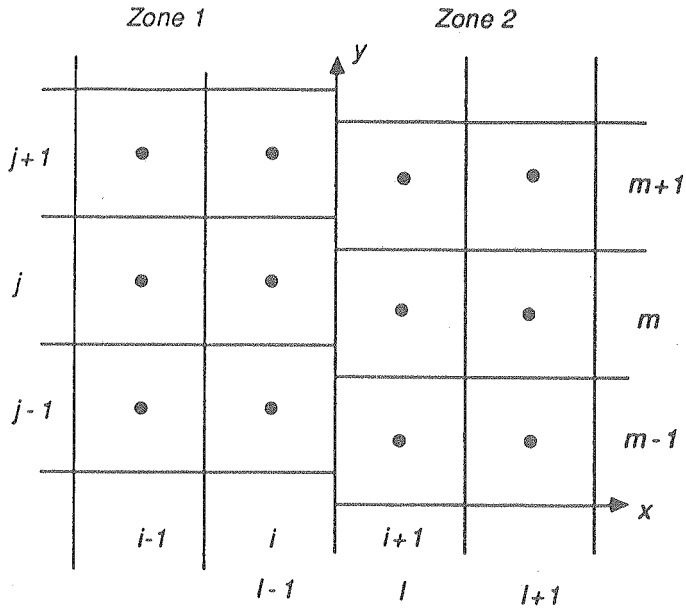

Figure 1. Two-dimensional zonal interface.

Defining the spatial flux in the x-direction as F, Rai [1] has demonstrated that global conservation can be maintained by enforcing spatial-flux conservation along the interface, as

$$\int F^{(1)}(x_{i+1/2})dy = \int F^{(2)}(x_{l-1/2})dy. \tag{4.1}$$

The flux in zone 2, say, is constructed from the flux in zone 1 so that (4.1) is satisfied. For a scheme requiring two points on either side of the interface to compute the flux, the flux in zone 1 can be constructed from the data in zone 1 and an interpolation of zone 2 data at a projection of zone 1 into zone 2. Referring to the conserved variables Q as the time flux of mass, momentum, and energy, much as F is referred to as the spatial flux of mass, momentum, and energy, the conservation of time flux in the region defined by the projected cells of zone 1 can be expressed as

$$\int\int Q^{(1)}dx\,dy = \int\int Q^{(2)}dx\,dy. \tag{4.2}$$

If it is assumed that the grid spacing normal to the interface boundary is nominally the same, then the dimension of the interpolation implied by (4.2) is reduced by one, to a form very much like (4.1). Under this assumption or for equal spacing in the x-direction, (4.2) becomes

$$\int Q^{(1)}(x_{i+1})dy = \int Q^{(2)}(x_l)dy. \tag{4.3}$$

If the spacing is not the same, the error introduced is equivalent to that introduced into a single grid by a step discontinuity in the spacing.

The flux in zone 1 could also have been constructed from zone 2 through (4.1), in which case a projection of zone 2 cells into zone 1 is required. The time-flux constraint equation counterpart of (4.3) is then

$$\int Q^{(2)}(x_{l-1})dy = \int Q^{(1)}(x_i)dy. \tag{4.4}$$

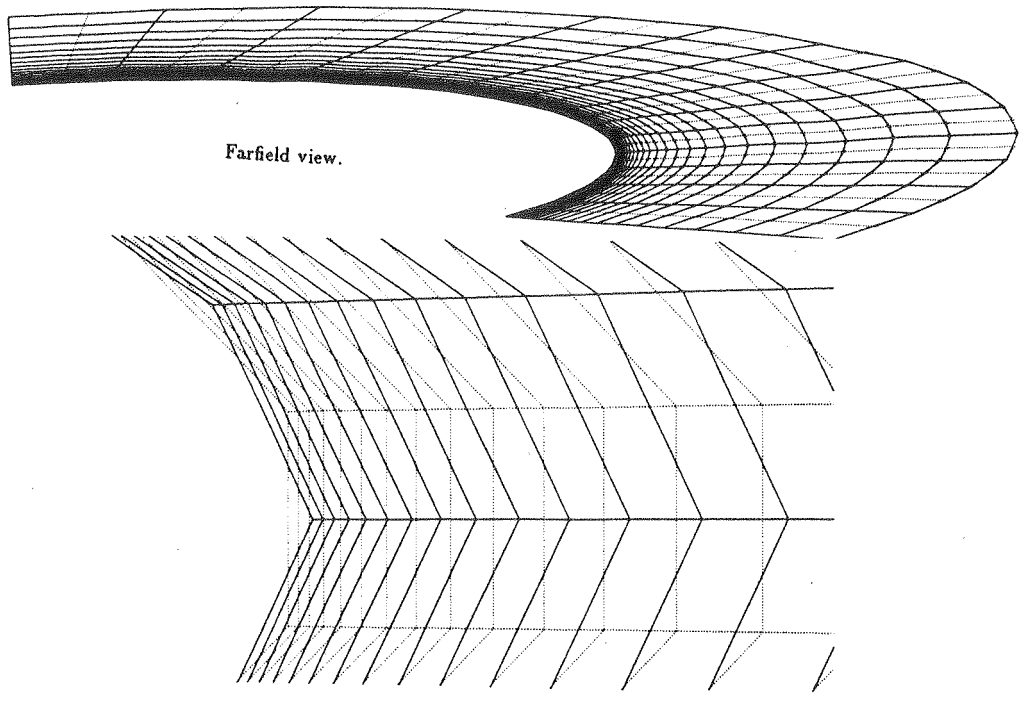

Figure 2. Zone 1 (solid lines) and Zone 2 (dotted lines) grids at the interface of a partial ellipse section.

The conservation relations for the redistribution of flux on one side of the interface onto the cell faces of the grid opposite the interface are expressed by (4.6) and (4.7). Defining the discrete flux in zone 1 to be interpolated at a particular location as $C^{(1)}_{j,k}$ from the discrete flux in zone 2, $C^{(2)}_{m,n}$, and assuming a piecewise constant variation of the flux, the interpolation reduces to determining the normalized area of overlap $N^{m,n}_{j,k}$ from the cells (m,n) of one zone onto the cells (j,k) of the other, i.e.

$$C^{(1)}_{j,k} = \sum_m \sum_n C^{(2)}_{m,n} N^{m,n}_{j,k}. \tag{4.8}$$

One approach to determining the area of overlap is a clipping algorithm, adapted from computer graphics, which has been used in the three-dimensional zonal calculations of [2], [3], and [5]. A more efficient procedure, originally developed for Lagrangian hydrodynamic rezoning calculations by Ramshaw [16], relies on the divergence theorem applied to the position vector to calculate the area as a summation of line integrals over the bounding polygons. For a linear mapping of the surface,

$$\vec{r} = \vec{a}_1 + \vec{a}_2\eta + \vec{a}_3\zeta, \tag{4.9}$$

the area of a cell A_p bounded by s directed line segments running from (η_1,ζ_1) to (η_2,ζ_2) is

$$A_p = \frac{|\vec{a}_2 \times \vec{a}_3|}{2} \sum_s \epsilon^p_s (\eta_1\zeta_2 - \eta_2\zeta_1), \tag{4.10}$$

where ϵ^p_s is either $+1$ or -1 as the cell p lies to the left or right, respectively, of the line segment s. The areas of overlap can be calculated by sweeping over the line segments of the two meshes, since all of the areas of overlap are formed by the intersection of mesh lines from the two surfaces. This procedure has been used in the three-dimensional calculations of Kathong et. al [6], Walters et. al [3], and Ghaffari et. al. [17]. The computational work for the area of overlap scales linearly with the number of mesh points. In a straightforward application, this procedure is more efficient than

Ideally, all of (4.1), (4.3), and (4.4) would be satisfied. However, any two of the three equations are sufficient to pass information between the zones. The approach which enforces (4.1) and either of (4.3) or (4.4), as in the work of Rai [1,5] and Walters et. al [2,3,8], is referred to as the spatial-flux conservation approach. The approach which enforces (4.3) and (4.4) is referred to as the time-flux conservation approach. There is some flexibility in the spatial flux approach in that the interpolation may be performed in a particular order. One would prefer to always interpolate from the finer mesh to the coarser mesh since the opposite order results in the fine mesh seeing the discontinuites on the coarse mesh. However, there are problems in which one mesh is finer than the other only in localized regions and coarser elsewhere. In these cases, the time-flux approach, which satisfies (4.1) only to within truncation error, has been found, in practice, to circumvent this difficulty and at the same time maintain the conservative, i.e. shock-capturing, properties of the single-zone scheme as well as the spatial-flux approach [7,8]. The time-flux approach arises naturally in rezoning techniques for Lagrangian or adaptive mesh simulations as well as in transferring information between grids in a multigrid calculation. For higher order spatial differencing, the above equations need to be augmented with relations representing the additional information required at the interface. For a four-point stencil at the interface, such as used in the present work, a minimum of four interpolations need to be done at an interface using either the spatial-flux or the time-flux appproach.

Viewing (4.2) as a conservative interpolation of the time fluxes at a projection of one zone into another, it is clear that the approach does not rely on the boundaries being coincident; hence, overlapped grids, such as that used in the Chimera scheme of Benek et. al [4], can be accomodated. Also, the time-flux approach eliminates the departure from freestream conditions that can occur near curved interfaces using the spatial-flux approach, because of the differences in the discrete boundary definitions of the two zones [8].

The counterpart in three dimensions of patching the zonal solutions along a line in two dimensions (Fig. 1) corresponds to patching along a surface. Given the three-dimensional coordinate transformation implied in (2.1) for each zone,

$$\vec{r} = \vec{r}(\xi, \eta, \zeta) \tag{4.5}$$

a patching surface can be defined without loss of generality as a surface of constant ξ. The patching algorithm must match the solution between the zones given the set of surface points on each grid defining the patching surface, as illustrated in Fig. 2 for a planar interface.

To interpolate across the interface, the transformation defined by the discrete ordered set of points in zone 1,

$$\{\vec{r}(\xi_i, \eta_j, \zeta_k) \quad : i = 1, i_{max};\ j = 1, j_{max};\ k = 1, k_{max}\},$$

is used to construct at the ξ = constant interface, the generalized coordinates for the set of points in zone 2 corresponding to the zonal boundary,

$$\{\vec{r}(\eta_m, \zeta_n; \xi) \quad : m = 1, m_{max};\ n = 1, n_{max}\}.$$

The equation to conserve the spatial flux at the ξ= constant interface is

$$\int\int \widehat{F}^{(2)} d\eta d\zeta = \int\int \widehat{F}^{(1)} d\eta d\zeta, \tag{4.6}$$

which is analagous to (4.1) for the two-dimensional case. Likewise, the counterpart to (4.2) is

$$\int\int\int \widehat{Q}^{(2)} d\xi d\eta d\zeta = \int\int\int \widehat{Q}^{(1)} d\xi d\eta d\zeta, \tag{4.7}$$

where the limits of integration span the cells adjacent to the interface. The spatial-flux conservation approach uses (4.6) and (4.7) to pass information across the boundary; the time-flux conservation approach uses (4.7) and an analagous equation for the projection of zone 1 into zone 2. For higher order differencing, (4.7) is augmented by a similar equation relating the conserved variables in the region spanned by the second set of cells in the ξ direction adjacent to the interface. The assumption of equal spacing across the interface reduces (4.7) to a two-dimensional equation.

the clipping approach [3] and was used for the inviscid calculations presented here about the SR71 aircraft.

The procedure used for the viscous simulations about the F/A-18 forebody was to interpolate to the cell centers of one grid assuming a linear variation of the flux within the cells of the other grid, as

$$\begin{aligned} C^{(1)}_{j,k} = C^{(2)}_{m,n} &+ (D_\eta C^{(2)})_{m,n}(\eta_j - \eta_m) \\ &+ (D_\zeta C^{(2)})_{m,n}(\zeta_k - \zeta_n), \end{aligned} \tag{4.11}$$

$$for\ \eta_{m-1/2} \le \eta_j \le \eta_{m+1/2},\ \zeta_{n-1/2} \le \zeta_k \le \zeta_{n+1/2},$$

where the slope in each zone can be determined to maintain monotonicity between the zones [14], as for example,

$$(D_\eta C^{(2)})_{m,n} = \frac{C^{(2)}_{m+1,n} - C^{(2)}_{m-1,n}}{\eta_{m+1,n} - \eta_{m-1,n}}\,\phi(r_{m,n}), \tag{4.12a}$$

$$\phi(r_{m,n}) = \frac{2r_{m,n}}{r^2_{m,n} + 1}, \tag{4.12b}$$

$$r_{m,n} = \frac{C^{(2)}_{m+1,n} - C^{(2)}_{m,n}}{C^{(2)}_{m,n} - C^{(2)}_{m-1,n}}. \tag{4.12c}$$

For both approaches, the geometric information describing the interpolation from one zone to another is calculated initially and then re-used at each subsequent iteration, so that the additional overhead due to the patching is minimal.

In order to construct the generalized coordinates of one zone given the discrete transformation defined by another zone, a local geometric variation is assumed in each cell. A bilinear variation in each cell,

$$\vec{r} = \vec{a}_1 + \vec{a}_2\eta + \vec{a}_3\zeta + \vec{a}_4\eta\zeta, \tag{4.13}$$

leads to a mismatch in the discrete boundary definition between the two grids near a curved boundary, as illustrated in Fig. 2. The boundary mismatch is not generally an issue for meshes encountered in computations for the Euler equations, since the mismatch is a small fraction of the area of the cells adjacent to the boundary. For solutions to the Navier-stokes equations, in which the grids are highly clustered near the boundary to resolve the viscous layers at high Reynolds numbers, the situation depicted is not uncommon.

The surface definition can be substantially improved by using a degenerate biquadratic fit in the direction tangential to the boundary, i.e.

$$\begin{aligned} \vec{r} = \vec{a}_1 &+ \vec{a}_2\eta + \vec{a}_3\zeta + \vec{a}_4\eta\zeta \\ &+ \vec{a}_5\eta^2 + \vec{a}_6\eta^2\zeta. \end{aligned} \tag{4.14}$$

This form ensures that the boundaries of the cells are continuous between the zones, if the grid point data is augmented by additional edge points in the η direction. For each ζ = constant cell edge, additional points are determined by passing a least squares quadratic curve through the 2 grid points defining a cell edge and the nearest grid point on either side. For the zones in Fig. 2, the grid mismatch is reduced from $O(1)$ to $O(10^{-2})$ wherein all the cell centers lie very close to midway between the grid points of the other. This approach works well for the case in which the nominal spacings in the two generalized coordinate directions are similar. For the more general case, it is necessary to obtain the coordinate normal to the surface by a local interpolation based on distance from each of the discrete boundary definitions.

The generalized coordinates of each cell center to be interpolated are determined through a nonlinear iterative procedure. A nearest enclosing cell is guessed based on the distance from the grid point data to the cell center and then updated by solving for (η, ζ) from (4.14) through a

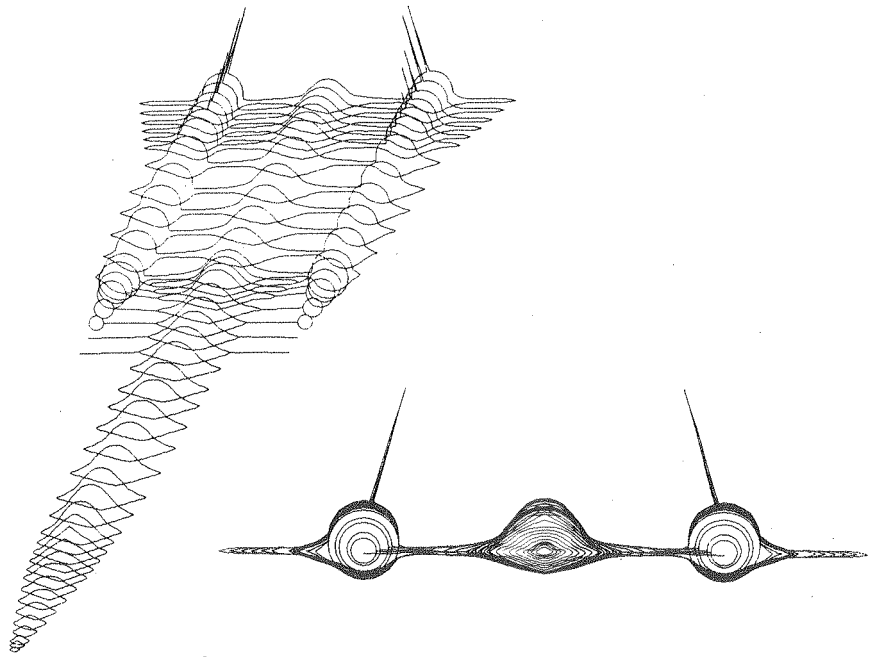

Figure 3. Simplified model of the SR71 aircraft.

Newton procedure, until the computed (η, ζ) lies within the candidate cell boundary. The conserved variables are then interpolated using the linear fit of (4.11).

5. Computational Results. In order to demonstrate the utility of domain decomposition via a multi-block approach, the flowfield about a relatively complete model of the SR71 reconnaissance aircraft (shown in Fig. 3) has been computed on a four block grid by the spatial flux conservation approach. Contours of pressure in the symmetry and exit plane for a Mach 3 calculation at atmospheric conditions corresponding to an altitude of 20 kilometers are shown in Fig. 4.

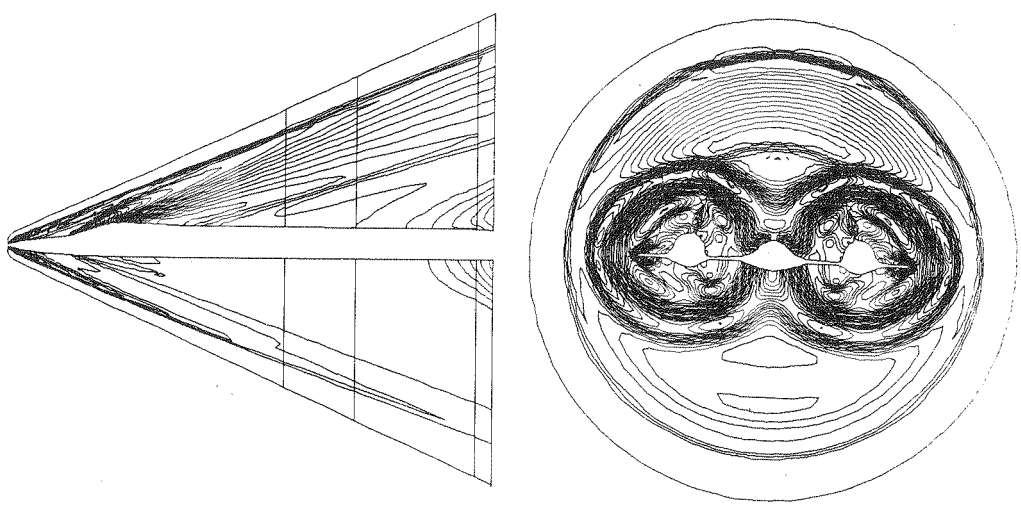

Figure 4. Symmetry and exit plane pressure contours from a 2^{nd} order calculation.

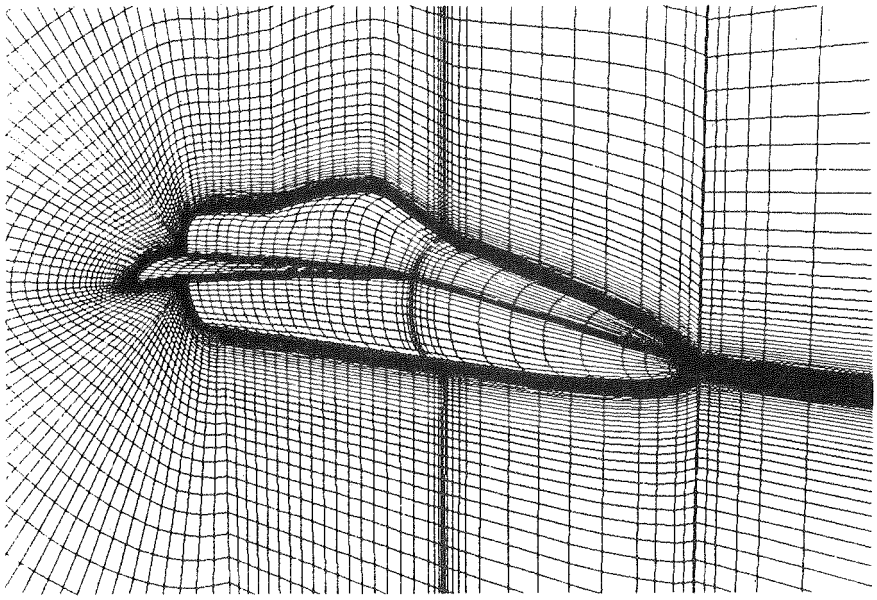

(a) Nearfield 2-block grid (185,000 points).

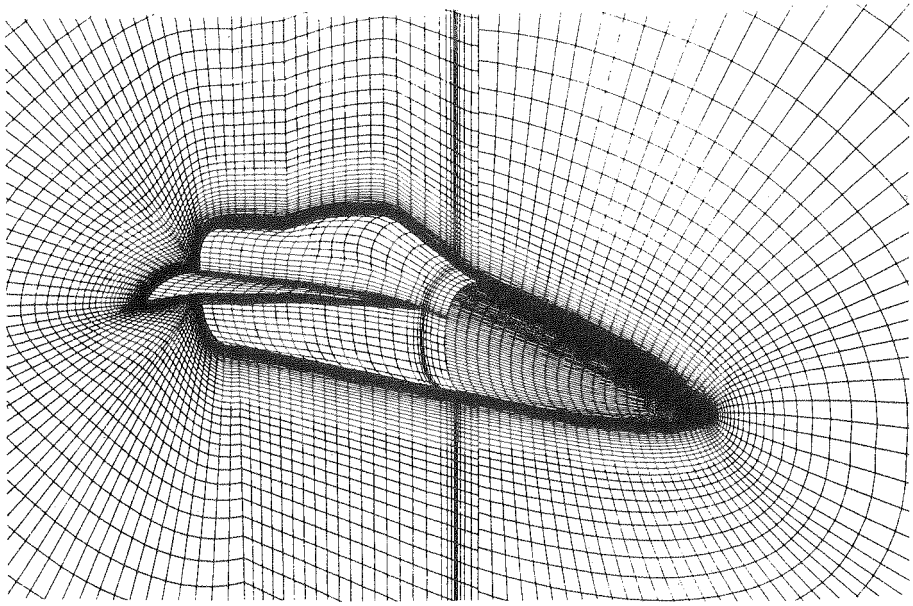

(b) Nearfield 3-block grid (300,000 points).

Figure 5. Grids for the F/A-18 forebody-strake.

The expected shock and expansion waves are clearly visible and there are no distortions along any of the vertical lines in the figure which are locations where the grids have been patched together.

The grid topologies used for the F/A-18 forebody-strake calculations are shown in Fig. 5. A 2-zone grid, shown in Fig. 5(a), is described in detail by Ghaffari et. al.[17]. The grids were generated in each block using an H-O topology with transfinite interpolation. The two blocks are patched together at the strake apex. The disadvantage of the 2-block grid topology is that the circumferential grid clustering at the strake propagates forward into and ahead of the nose region. A three-block grid is shown in Fig. 5(b). Part of the upstream block in Fig. 5(a) is replaced with an O-O topology. The additional block gives a much better resolution of the forebody geometry; the additional zonal interface is evident on the body surface and in the longitudinal plane of symmetry.

Symmetry plane pressure contours using the spatial-flux and time-flux conservation strategies for the 2-block grid are shown in Fig. 6 for the conditions considered in [17]: laminar flow at $M_\infty = 0.6, R_{\bar{c}} = 0.8 \times 10^6, \alpha = 20$ deg. Both calculations interpolate across the zonal interface using (4.8) and (4.10). The two solutions are nominally the same; any differences are on the order of the truncation error of the calculations.

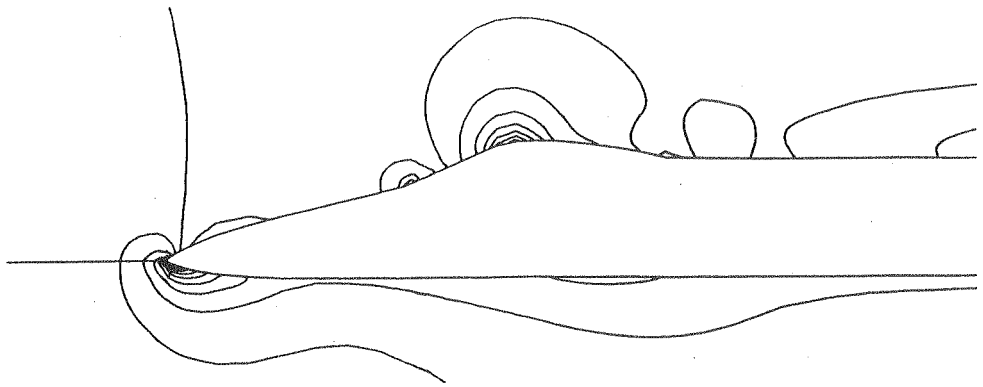

(a) Spatial-flux conservation.

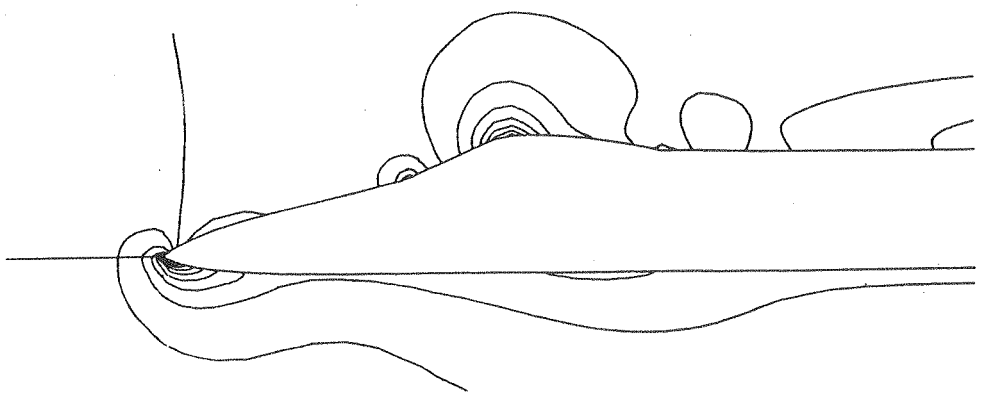

(b) Time-flux conservation.

Figure 6. Centerline pressure contours, $M_\infty = 0.6,\ \alpha = 20°$

Computed total pressure contours and surface particle traces are shown in Fig. 7 at a high angle-of-attack, laminar flow condition: $M_\infty = 0.3, R_{\bar{c}} = 0.74 \times 10^6, \alpha = 30$ deg. The primary and secondary separation lines on the forebody are evident, as well as the secondary separation line on the strake. The vortices shed along these lines are very shallow and lie close to the body surface, especially in comparison to the primary vortex shed from the strake. The primary separation line on the forebody leads into a large region of reverse flow ahead of and predominantly under the strake apex. Under the strake along the body, a primary separation line is evident, leading to a vortex impinging on the strake lower surface. Along the fuselage above the strake, a separation line extending downstream from the apex is evident. The streamlines pass smoothly through the zonal interfaces.

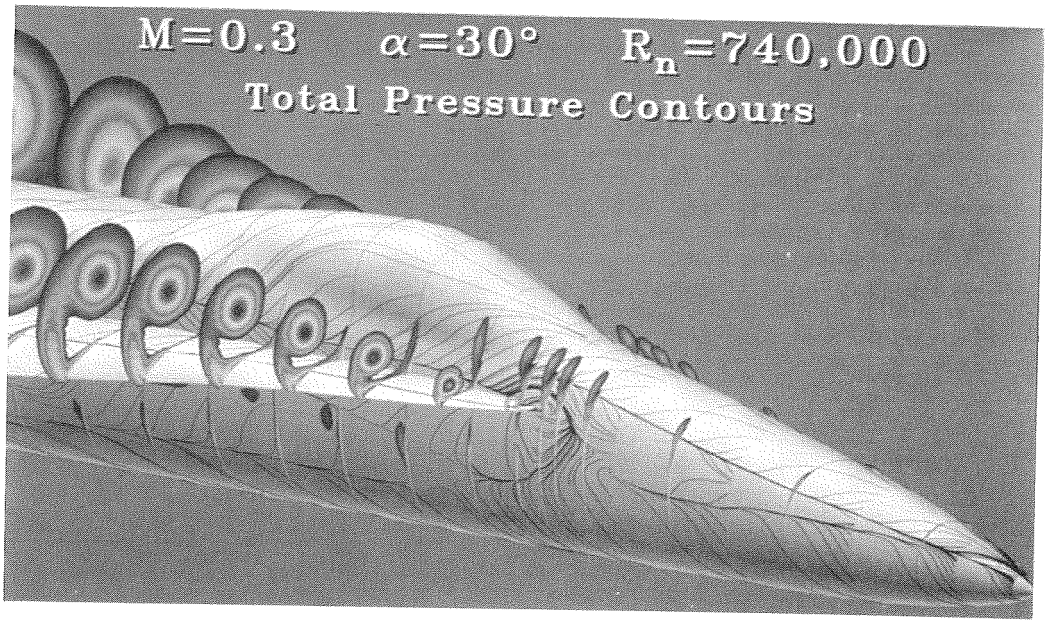

Figure 7. Total pressure contours and surface particle traces for the forebody-strake.

Oil flows from a test in the Basic Aerodynamics Research Tunnel (BART) [18] at NASA Langley Research Center for the same angle of attack but at a slightly lower Reynolds number have been compared to the computed particle traces in [19] and demonstrate a striking resemblance to the computations. In addition, comparisons with flight-test results [20] at turbulent flow conditions are also presented by the authors in [19].

6. Concluding Remarks. A patched grid algorithm for complex configurations has been described. The work is an extension to the longitudinally-patched approach of [2,3], allowing for the analysis of grids which are highly stretched in the normal direction to resolve viscous flows, and for arbitrarily-shaped patch surfaces. Two algorithms, a spatial-flux and a time-flux conservation approach, have been used across zonal interfaces with few differences noted. The latter approach is somewhat more flexible and can be easily extended to handle more complex situations, such as overlapped and embedded grids. A longer term objective of the present domain decomposition approach is for the only constraint on the grid topology to be that the grids span the entire physical domain. The computational algorithm should be general enough to automatically determine the necessary connections between the domains to ensure a globally second-order accurate solution.

REFERENCES

[1] M.M. Rai, *A Relaxation Approach to Patched-Grid Calculations with the Euler Equations,* AIAA Paper. No. 85-0295, 1985.

[2] R.W. Walters, T. Reu, W.D. McGrory, J.L. Thomas, and P.F. Richardson, *A Longitudinally-Patched Grid Approach with Applications to High Speed Flows,* AIAA Paper No. 88-0715, 1988.

[3] R.W. Walters, T. Reu, J.L. Thomas, and W.D. McGrory, *Zonal Techniques for Flowfield Simulation About Aircraft,* ASME Symposium on Advances and Trends in Computational Structural Mechanics and Fluid Dynamics, Washington, D.C., October 1988.

[4] J.A. Benek, P.G. Buning, and J.L. Steger, *A 3-D Chimera Grid Embedding Technique,* AIAA Paper No. 85-1523CP, 1985.

[5] K.A. Hessinius and M.M. Rai, *Three Dimensional, Conservative, Euler Computations Using Patched Grid Systems and Explicit Methods,* AIAA Paper No. 86-1081, 1986.

[6] M. Kathong, R.E. Smith, and S.N. Tiwari, *A Conservative Approach for Flow Field Calculations on Multiple Grids,* AIAA Paper No. 88-0224, 1988.

[7] J.L. Thomas, D.H. Rudy, S.R. Chakravarthy, and R.W. Walters, *Patched-Grid Computations of High-Speed Inlet Flows,* Symposium on Advances and Applications in Computational Fluid Dynamics, Chicago, Illinois, ASME FED Vol. 66, 1988, pp. 11-22.

[8] R.W. Walters, J.L. Thomas, and G.F. Switzer, *Aspects and Applications of Patched Grid Calculations,* AIAA Paper No. 86-1063, 1986.

[9] B.S. Baldwin and H. Lomax, *Thin Layer Approximation and Algebraic Model for Separated Turbulent Flows,* AIAA Paper No. 78-257, 1978.

[10] D. Degani and L.B. Schiff, *Computation of Supersonic Viscous Flows Around Pointed Bodies at Large Incidence,* AIAA Paper No. 83-0034, 1983.

[11] V.N. Vatsa, J.L. Thomas, and B.W. Wedan, *Navier-Stokes Computations of Prolate Spheroids at Angle of Attack,* AIAA Paper No. 87-2627-CP, 1987.

[12] P.L. Roe, *Characteristic Based Schemes for the Euler Equations,* Annual Review of Fluid Mechanics, 1986, pp. 337-365.

[13] B. Van Leer, J.L. Thomas, P.L. Roe, and R.W. Newsome, *A Comparison of Numerical Flux Formulas for the Euler and Navier-Stokes Equations,* AIAA Paper No. 87-1104CP, 1987.

[14] B. Van Leer, *Upwind-Difference Methods for Aerodynamic Flows Governed by the Euler Equations,* Lectures in Applied Mathematics, Vol. 23, Part 2, AMS, Providence, 1985, pp. 327-336.

[15] W.K. Anderson, J.L. Thomas, and B. Van Leer, *Comparison of Finite-Volume Flux-Splitting Methods for the Euler Equations,* AIAA Journal, Vol. 24, No. 9, 1986, pp. 1453-1460.

[16] J.D. Ramshaw, *Conservative Rezoning Algorithms for Generalized Two-Dimensional Meshes,* Journal of Computational Physics, Vol. 59, 1985, pp. 193-199.

[17] F. Ghaffari, J.M. Luckring, J.L. Thomas, and B.L. Bates, *Navier-Stokes Solutions About the F/A-18 Forebody-LEX Configuration,* AIAA Paper No. 89-0338, 1989.

[18] W.L. Sellers III and S.O. Kjelgaard, *The Basic Aerodynamics Research Tunnel - A Facility Dedicated to Code Validation,* AIAA Paper No. 88-1997CP, 1988.

[19] J.L. Thomas, R.W. Walters, T. Reu, F. Ghaffari, R.P. Weston, and J.M. Luckring, *A Patched-Grid Algorithm for Complex Configurations Directed Towards the F/A-18 Aircraft,* AIAA Paper No. 89-0121, 1989.

[20] D.F. Fisher and R.R. Meyer Jr. *Flow Visualization Techniques for Flight Research,* NASA TM 100455, October, 1988.